

February 5, 2001

A Compilation of High Energy Atmospheric Muon Data at Sea Level

Thomas Hebbeker

Institut für Physik der Humboldt-Universität zu Berlin,
Invalidenstr. 110, D-10115 Berlin, Germany

Charles Timmermans

Katholieke Universiteit Nijmegen,
Toernooiveld 1, N-6525 ED Nijmegen, Netherlands

ABSTRACT

We collect and combine all published data on the vertical atmospheric muon flux and the muon charge ratio for muon momenta above 10 GeV. At sea level the world average of the momentum spectra agrees with the flux calculated by E.V. Bugaev et al. within 15 %. The observed shape of the differential flux versus momentum is slightly flatter than predicted in this calculation. The experimental accuracy varies from 7% at 10 GeV to 17% at 1 TeV. The ratio of fluxes of positive to negative muons is found to be constant, at a value of 1.268, with relative uncertainties increasing from approximately 1% at low momenta to about 6% at 300 GeV.

1. Introduction

We collect measured atmospheric muon flux data and charge ratios as a function of momentum and compute world averages. Only measurements at sea level or low altitudes and for (near) vertical incidence are taken into account, since several data sets are available for these experimental conditions. Here we consider only data with muon momenta above 10 GeV. At lower momenta geomagnetic effects and solar influences play a significant role and make the interpretation of the data more difficult. A recent compilation of charge ratio data at low muon momenta can be found in reference [1].

A precise knowledge of the muon spectrum and charge ratio allows to constrain the primary flux and the models of atmospheric showers so that also the atmospheric neutrino fluxes can be calculated with a good precision. This is a very important issue, since the Superkamiokande experiment[2] and others have seen indications for a disappearance of atmospheric muon neutrinos. So far this interpretation is based on the angular distribution and on the ratio of muon neutrino to electron neutrino fluxes. It is very important to compare also directly the measured and calculated absolute muon neutrino fluxes; until now this was prevented by the large model uncertainties.

2. Effects relevant for spectrum and charge ratio

The following effects might influence the measurements of the muon flux and the charge ratio. It is possible that the published data need to be corrected accordingly in order to arrive at a meaningful comparison between the various measurements.

- Geomagnetic effects

For near vertical incidence the geomagnetic cutoff for primary protons is below 10 GeV for all latitudes at which the cosmic ray measurements were made[3] (exceptions are discussed below). Geomagnetic effects can therefore be neglected.

- Solar modulation

Using the parameterization given in reference [4] we estimate that the primary proton flux at 50 GeV (100 GeV) decreases by 3% (1.6 %) at maximum solar activity compared to the minimum. The mean primary proton momentum resulting in 10 GeV muons at sea level exceeds 100 GeV. Using the air shower program CORSIKA [5], we found that about 80% of those protons have a momentum larger than 50 GeV. This results in an uncertainty of $\pm 1\%$ for the muon flux at a momentum of 10 GeV. Similarly, one can estimate a flux uncertainty of $\pm 0.5\%$ at 20 GeV and less at higher momenta. At 10 GeV the charge ratio is expected to change by about $\pm 0.2\%$. At higher momenta the effect is even smaller. We do *not* correct the data for time dependent solar effects.

- Altitude dependence

Not all experiments measure at sea level. In order to investigate the dependence of flux and charge ratio on the altitude we used the air shower simulation program CORSIKA and also apply the empirical formula found by De Pascale et al.[6].

For muon momenta above 10 GeV and altitudes less than about 1000 m the vertical muon flux can be parameterized by

$$\frac{\Phi(h)}{\Phi(h=0)} = e^{h/L} \pm 0.003 \quad (1)$$

where h = altitude, $L = 4900 \text{ m} + 750 \text{ m} \frac{p}{\text{GeV}}$ and p = muon momentum.

The form of the parameterization is similar to the one used in[6]. The uncertainty of ± 0.003 reflects the quality of the parameterization and the comparison to the measurements. Example: For $h = 1000 \text{ m}$ and $p = 10 \text{ GeV}$ we obtain the flux $\Phi(h) = 1.08 \cdot \Phi(h = 0)$. Note: Caprice data[7] disagree with both [6] and CORSIKA for higher momenta; here they have not been taken into account.

The charge ratio is not affected, it changes by less than 0.005 for $h < 1000 \text{ m}$ and $p > 10 \text{ GeV}$.

We do correct all published fluxes using formula (1).

- Zenith angle dependence

The muon data are normally collected within a certain cone around the vertical direction, including zenith angles up to θ^{max} . With help of CORSIKA we find that the zenith angle dependence can be parameterized in the form

$$\frac{d\Phi}{d\cos\theta} \sim 1 + a(p) \cdot (1 - \cos\theta) \quad (2)$$

with a momentum dependent coefficient $a(p)$. Accordingly we estimate the following flux reduction factors

$$g(\theta) = \frac{d\Phi}{d\cos\theta}(\theta) / \frac{d\Phi}{d\cos\theta}(0) \quad (3)$$

p/GeV	a	$g(5^\circ)$	$g(10^\circ)$	$g(20^\circ)$
10	-1.50	0.994	0.978	0.910
30	-1.28	0.995	0.981	0.925
100	-0.94	0.996	0.986	0.944
300	-0.61	0.998	0.991	0.963
1000	-0.22	0.999	0.997	0.987

Note: the entries are differential values, they have not been integrated over θ .

Since not all experiments quote the range of accepted zenith angles, we *cannot* correct for this effect. We have to keep in mind that this might cause a bias, especially at low momenta.

- Atmospheric pressure/temperature profile

Previous calculations[8] and measurements[9] indicate that the relative muon flux variation $\Delta\Phi$ at ground level is related to the temperature-distribution in the atmosphere via

$$\frac{\Delta\Phi}{\Phi} = \alpha \cdot \frac{\Delta T_{eff}}{T_{eff}} \quad (4)$$

Φ is the integral flux above a certain muon momentum threshold p_{th} . T_{eff} is the absolute effective temperature of the higher atmosphere. α is the temperature coefficient, which is a function of zenith angle and muon energy. For zenith angles $\theta \approx 0$ [8, 9]:

$$\alpha = \left[1 + \frac{70 \text{ GeV}}{p_{th}} \right]^{-1} \quad (5)$$

Simulations using CORSIKA arrive at similar conclusions. Example: At a threshold of 70 GeV the formula yields $\alpha = 0.5$. Since the atmospheric temperature, with a typical value of 220 K, varies over the year by up to ± 5 K, this implies a flux change of $\pm 1\%$.

For muon momenta above 10 GeV the pressure at ground level is not expected to show a significant correlation with the flux[8].

Unfortunately, most experiments do not report the atmospheric temperature, nor do they correct for this effect. It is even not clear, how to define the reference value. Therefore, we *cannot* correct for atmospheric effects.

- Unfolding of the momentum spectrum

The measured muon spectrum agrees with the true spectrum only if the momentum resolution is small compared to the momenta being investigated. Otherwise, the steepness of the spectrum, which falls off approximately according to

$$\frac{d\Phi}{dp} \sim p^{-3} \quad (6)$$

leads to an asymmetric distortion, an enhancement of the measured flux at high momenta. Thus, the measured spectrum needs to be unfolded for experimental resolution effects. In the most simple approach - assuming the spectrum is roughly known - this can be achieved by a simple correction factor, which has been calculated in [10]. The authors assume the spectrum (6) and a Gaussian error distribution in the variable $1/p$ with width $\sigma_{1/p}$. Often the experimental resolution is given in terms of the ‘Maximum Detectable Momentum’ p_{MDM} , defined as the momentum value for which the integral over the Gauss distribution becomes 1/2:

$$E\left(\frac{1/p_{MDM}}{\sqrt{2}\sigma_{1/p}}\right) = \frac{1}{2} \quad \text{with} \quad E(x) \equiv \frac{2}{\sqrt{\pi}} \int_0^x e^{-t^2} dt \quad (7)$$

Thus,

$$\frac{1}{p_{MDM}} = 0.6745 \sigma_{1/p} \quad (8)$$

The ratio of the measured and true spectra is then given by

$$R\left(\frac{p_{MDM}}{p}\right) = E\left(0.4769 \frac{p_{MDM}}{p}\right) + 1.1829 \frac{p}{p_{MDM}} \exp\left(-0.2275 \frac{p_{MDM}^2}{p^2}\right) \quad (9)$$

The measured flux must be multiplied by $1/R$ to correct for the experimental resolution. Figure 1 shows the dependence of R on $1/p$. For $p < 0.3 p_{MDM}$ the correction amounts to less than 1% and can be neglected. For higher momenta the correction rises strongly and must be taken into account.

We have assumed that the experimenters have corrected their data for momentum resolution effects or that they can be neglected. However, several papers are not very clear on this point. Therefore, some published spectra might be biased towards too high flux values at large momenta.

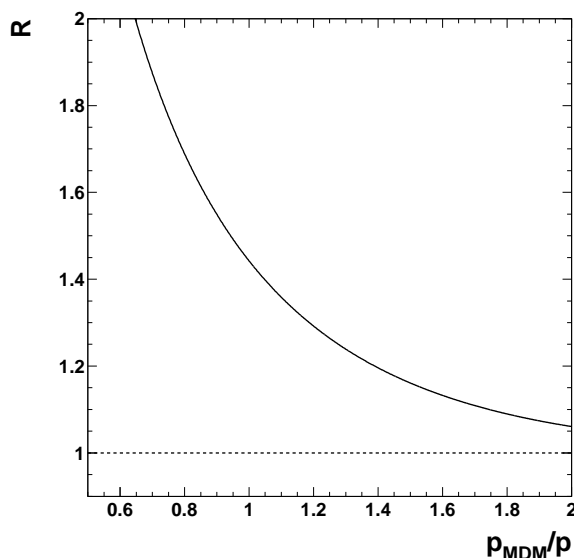


Figure 1: Unfolding correction factor

3. Experimental Data

Only published results are taken into account. In appendix A we summarize the characteristics of all relevant experiments/publications, in chronological order. The spectrum and charge ratio data used in this compilation are listed explicitly in appendices B and C.

4. Absolute muon flux

There are two aspects to the measurement of the absolute muon flux, namely the shape of the spectrum as a function of energy and the absolute normalization. Some experiments only measure the relative muon flux as a function of momentum. Therefore we will analyze the data in two steps. First we check the spectral shape, leaving the normalization as a free parameter. Secondly we determine the absolute normalization of the spectrum.

4.1 The shape of the muon spectrum

A whole range of experiments are performed to measure the muon flux, the measurements used are listed in appendix B. We have corrected the datasets for altitude, which is a small correction in most cases. In order to be able to compare the datasets, we fit each set to a reference shape, using the data with momenta above 10 GeV. In this fit, and in the following, we assume that the measurement performed in each momentum bin is independent of the other momentum bins. The reference shape is taken from the theoretical calculation by Bugaev et al [11], leaving the normalization as a free parameter. In general this shape provides a good description of the datasets, as can be seen below. The results of our fit are listed in table 1. In this table, we separated the data from Rastin[25] into two sets, as different normalizations are used in their paper. Next to fitting the normalization, we also calculated the normalization by comparing the integrated flux above 10 GeV/c (or the lower cutoff of the experiment whichever is higher) to an integrated flux calculation using the reference shape. The data published in references [13], [16] and [15] do not allow for this normalization method. As these papers are normalized

Data set	χ^2/NDF	Normalization from fit	Normalization from integration
Caro 1950 [12]	2.6/4	0.65 ± 0.03	0.74 ± 0.09
Owen 1955 [13]	0.5/2	0.819 ± 0.013	0.829
Pine 1959 [14]	4/11	0.76 ± 0.03	0.76
Pak 1961 [15]	4/6	0.75 ± 0.03	0.76
Holmes 1961 [16]	43/12	0.807 ± 0.016	0.829
Hayman 1962 [17]	13/14	0.735 ± 0.007	0.746 ± 0.008
Aurela 1967 [18]	0.7/2	0.81 ± 0.03	0.79 ± 0.03
Appleton 1971 [19]	38/23	0.370 ± 0.003	0.366 ± 0.003
Allkofer 1971 [20]	116/8	1.058 ± 0.006	1.01 ± 0.01
Bateman 1971 [21]	8/8	0.871 ± 0.008	0.83 ± 0.03
Nandi 1972 [22]	60/14	0.998 ± 0.008	1.001 ± 0.008
Ayre 1975 [23]	348/44	0.980 ± 0.002	0.95 ± 0.02
Green 1979 [24]	2.3/4	0.98 ± 0.02	0.98 ± 0.02
Rastin 1984 [25] (10-25 GeV)	0.2/5	0.995 ± 0.003	0.977 ± 0.002
Rastin 1984 [25] (>25 GeV)	24/29	0.960 ± 0.005	0.951 ± 0.005
De Pascale 1993 [6]	7/5	0.798 ± 0.016	0.80 ± 0.03
Tsuji 1998 [26]	16/13	0.961 ± 0.014	0.972 ± 0.014
Kremer 1994 data [27]	10/6	0.822 ± 0.009	0.818 ± 0.007
Kremer 1997 data [27]	13/6	0.831 ± 0.008	0.821 ± 0.007

Table 1: Normalization of datasets with respect to the Bugaev calculation

to Rossi [28] we recalculate this normalization point with the reference shape. The data of [21] are normalized to the differential flux at 10 GeV/c. The results of this calculation are shown in the last column of table 1. In general, both normalizations are in good agreement.

The high energy part of the Rastin data is shown in figure 2. Here and in the following we present all spectra weighted with p^3 , a common practice to compensate for the steep fall-off with momentum. Figure 2 nicely shows that the reference shape fits the data rather well, which justifies the use of the Bugaev curve as a reference. However, the data has the tendency to be slightly higher than the normalized curve at the higher momentum values.

The χ^2 of the fit as listed in this table made us re-check five datasets; the first four are shown in figure 3. The data of Holmes[16] clearly show that a simple re-normalization will not work. The data points do not follow the reference shape, especially at higher momenta. In their paper Holmes et al. apply additional corrections to the highest two data points, indicating that these are close to the MDM of the detector. Unfortunately, the value of this maximal momentum is not mentioned.

The Appleton data[19] are scattered a lot around the curve. With the value of χ^2/NDF being only slightly less than 2, this plot suggests that the errors could be underestimated.

The Allkofer data[20] have a completely different shape. The data rise faster than the reference shape and plateau at a lower value. This plateau also seems to be wider than suggested by the reference distribution.

The Nandi data[29] rise to a significantly higher value than predicted by the reference shape. This and the low value of the third data point create the large χ^2 .

The Ayre data[23] (left side of fig. 4) start off below the curve and continue to rise longer than

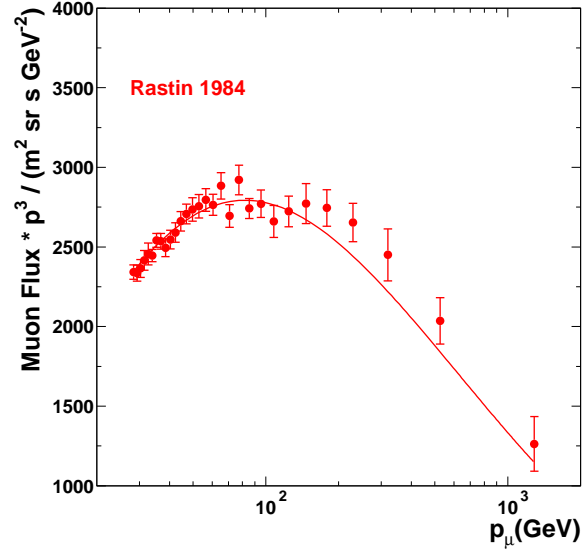


Figure 2: Muon flux data by Rastin et al.[25] in comparison to the reference spectrum from Bugaev et al.[11], after normalization

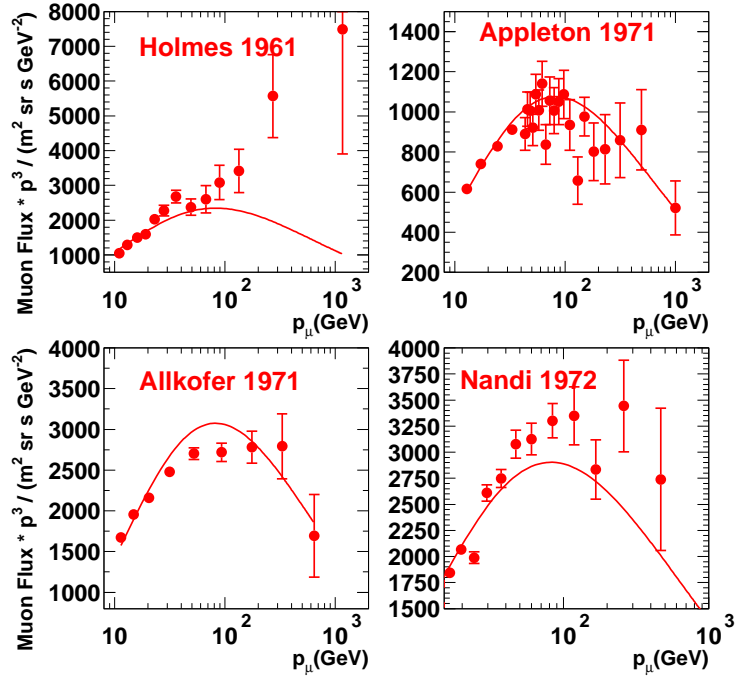


Figure 3: Muon flux data by Holmes et al.[16], Appleton et al.[19], Allkofer et al.[20] and Nandi et al.[29] in comparison to the reference spectrum from Bugaev et al.[11], after normalization

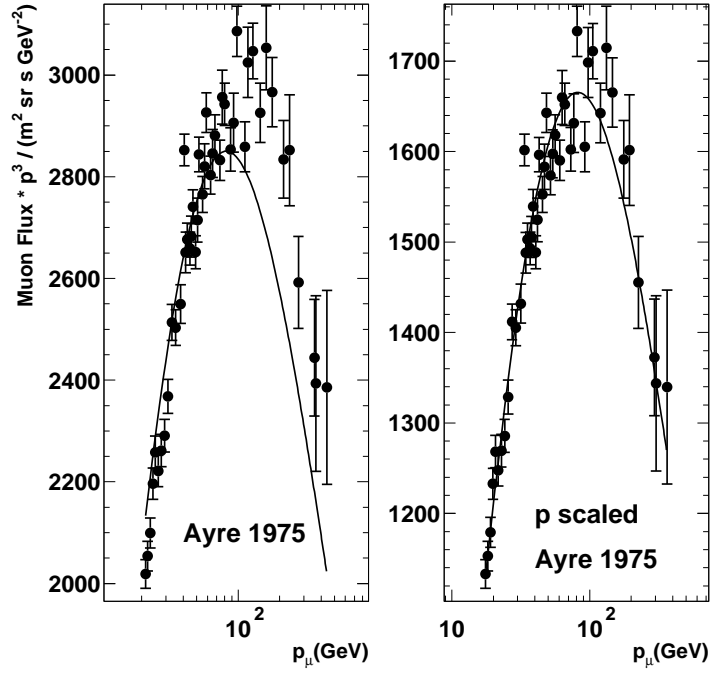


Figure 4: Muon flux data by Ayre et al.[23] in comparison to the reference spectrum from Bugaev et al.[11], after normalization. Left: data as published. Right: spectrum after momentum scaling.

expected. Therefore, the peak is at a higher value, but the drop-off rate seems to be similar as predicted on a $\log(p)$ scale. The curve suggests that the momentum could be over-estimated. A best fit of the momentum scale leads to a scaling of the momenta by a factor of 0.825, see right side of fig. 4. The χ^2/NDF improves from 348/44 to 136/44. It naturally changes the normalization. The muon spectrum closely follows a p^{-3} -dependence, thus the normalization is changed to about 56 % of the original. This is in fact what we observe. Even using the modified momentum, for which we cannot find a justification, the Ayre data do not fit the curve very well.

If we ignore these five datasets for the moment, we can compare the remaining data to the reference curve. We do this by applying the normalization calculated as outlined before, and listed in table 1 as ‘normalization from integration’. The result is shown in figure 5. The top

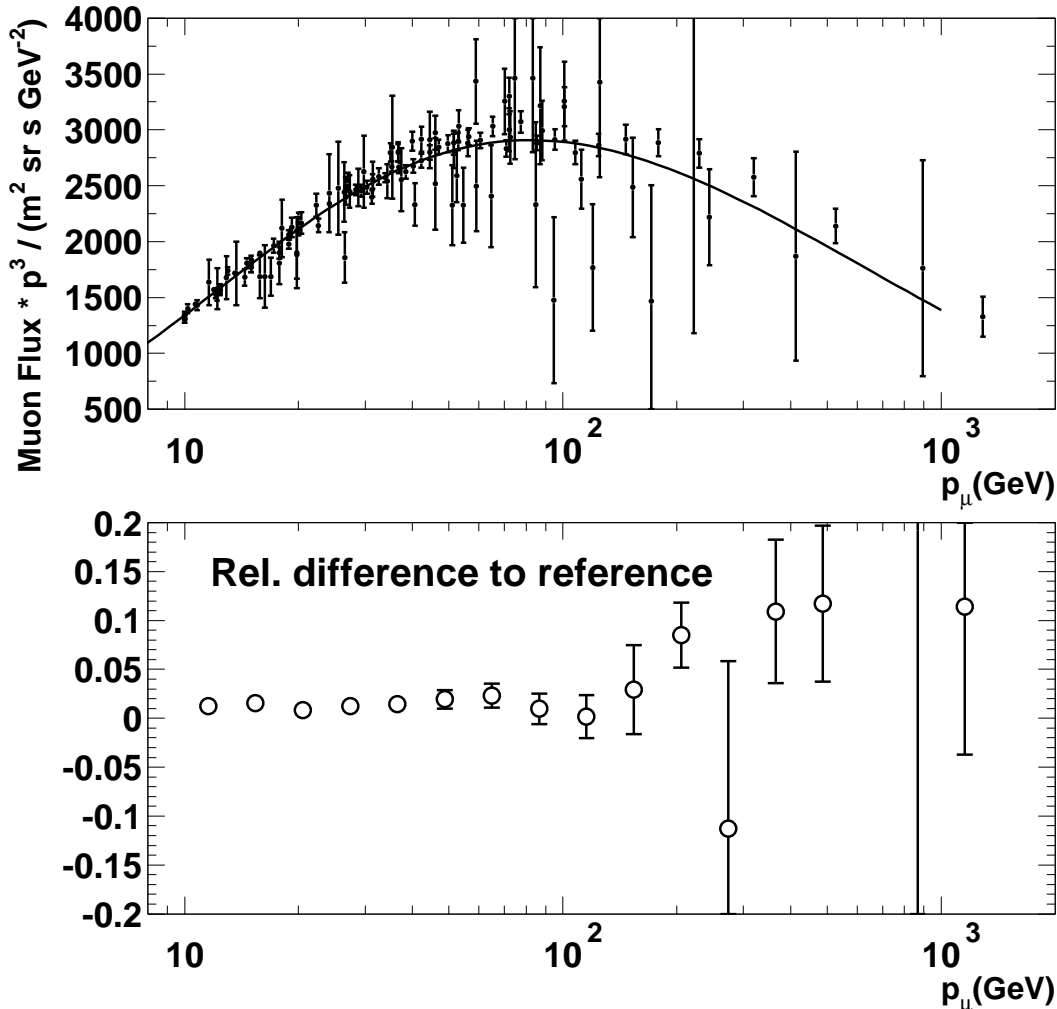


Figure 5: ‘Good’ data in comparison to reference spectrum.

part of this plot shows a direct comparison of all the datasets to the theory, while the bottom part shows the relative difference between these measurements and the description. The larger differences at higher momenta are mainly due to the data by Rastin et al. [25]. If we include

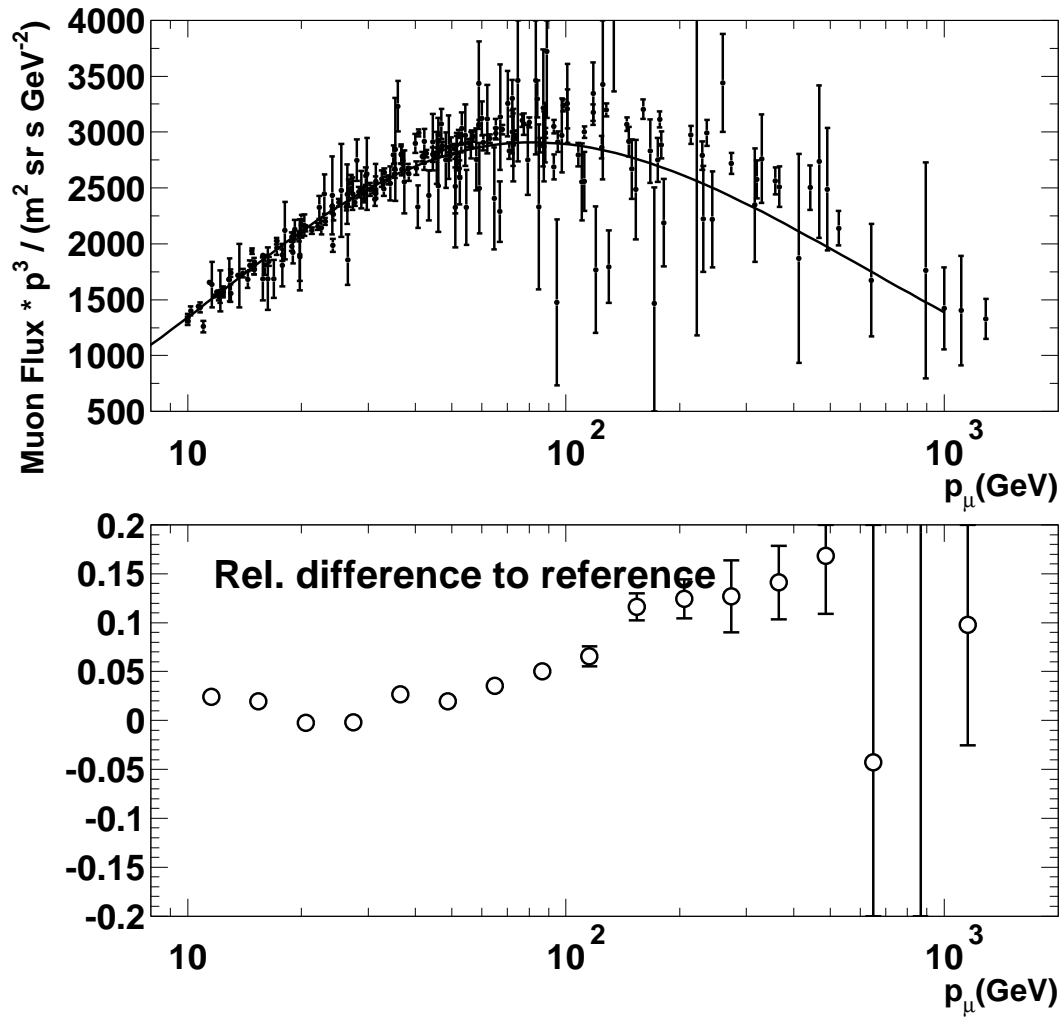


Figure 6: All data in comparison to reference spectrum.

the remaining five datasets the difference between the shape of the data and the reference shape increases, especially at higher momenta. This can be seen in figure 6.

The relative differences are plotted in 8 bins per decade, equidistant in $\log(p)$. This choice represents a good compromise taking into account experimental uncertainties and the rate of change of the p^3 -weighted spectrum with momentum. The χ^2/NDF values and the average flux values in the units $\text{m}^{-2} \text{sr}^{-1} \text{s}^{-1} \text{GeV}^{-1}$ are shown for each bin in table 2. The five datasets

p bin	p/GeV	good set		all data	
		χ^2/NDF	Flux	χ^2/NDF	Flux
1	11.5	19/15	$9.88 \cdot 10^{-1}$	129/20	1.00
2	15.4	11/12	$5.09 \cdot 10^{-1}$	40/17	$5.11 \cdot 10^{-1}$
3	20.5	20/14	$2.49 \cdot 10^{-1}$	36/21	$2.46 \cdot 10^{-1}$
4	27.4	19/16	$1.19 \cdot 10^{-1}$	76/27	$1.17 \cdot 10^{-1}$
5	36.5	22/14	$5.49 \cdot 10^{-2}$	85/22	$5.56 \cdot 10^{-2}$
6	48.7	12/15	$2.47 \cdot 10^{-2}$	45/31	$2.47 \cdot 10^{-2}$
7	64.9	14/11	$1.08 \cdot 10^{-2}$	33/23	$1.09 \cdot 10^{-2}$
8	86.6	8/8	$4.52 \cdot 10^{-3}$	48/19	$4.70 \cdot 10^{-3}$
9	115	10/6	$1.86 \cdot 10^{-3}$	51/12	$1.98 \cdot 10^{-3}$
10	154	2.4/2	$7.78 \cdot 10^{-4}$	18/9	$8.44 \cdot 10^{-4}$
11	205	0.3/2	$3.27 \cdot 10^{-4}$	10/6	$3.39 \cdot 10^{-4}$
12	274	0/0	$1.05 \cdot 10^{-4}$	12/4	$1.33 \cdot 10^{-4}$
13	365	0.3/1	$5.03 \cdot 10^{-5}$	0.6/4	$5.18 \cdot 10^{-5}$
14	487	0/0	$1.91 \cdot 10^{-5}$	1.1/3	$2.00 \cdot 10^{-5}$
15	866			0/0	$6.08 \cdot 10^{-6}$
16	1155	0/0	$2.76 \cdot 10^{-5}$	0/0	$2.76 \cdot 10^{-7}$
17	1540	0/0	$9.23 \cdot 10^{-7}$	3/3	$9.10 \cdot 10^{-8}$
18	2054				

Table 2: Average flux in $\text{m}^{-2} \text{sr}^{-1} \text{s}^{-1} \text{GeV}^{-1}$

discussed above have a large impact on the χ^2 of the relative difference in these bins. Therefore, we will exclude them when adjusting the shape according to the measurements. We fit a third degree polynomial to the logarithm of the flux as a function of the logarithm of momentum. We parameterize this function as follows:

$$\begin{aligned}
H(y) &= H_1 \cdot (y^3/2 - 5y^2/2 + 3y) \\
&\quad + H_2 \cdot (-2y^3/3 + 3y^2 - 10y/3 + 1) \\
&\quad + H_3 \cdot (y^3/6 - y^2/2 + y/3) \\
&\quad + S_2 \cdot (y^3/3 - 2y^2 + 11y/3 - 2) \\
y &= {}^{10}\log(p/\text{GeV}) \\
F(p) &= 10^{H(y)} \text{m}^{-2} \text{sr}^{-1} \text{s}^{-1} \text{GeV}^{-1}
\end{aligned} \tag{10}$$

This parameterization is similar to the one used by [11], however the fit variables are chosen such that they have a simple interpretation: H_1 , H_2 , and H_3 represent the logarithm of the differential flux at 10, 100 and 1000 GeV, S_2 represents the exponent of the differential flux at 100 GeV. The χ^2/NDF of this fit is 8/12, the correlation matrix is shown in appendix D. The fitted parameters are listed below, as well as the equivalent values from our reference shape.

	H_1	H_2	H_3	S_2
Reference	0.127	-2.539	-5.86	-2.00
Fit	0.135 ± 0.002	-2.529 ± 0.004	-5.76 ± 0.03	-2.10 ± 0.03

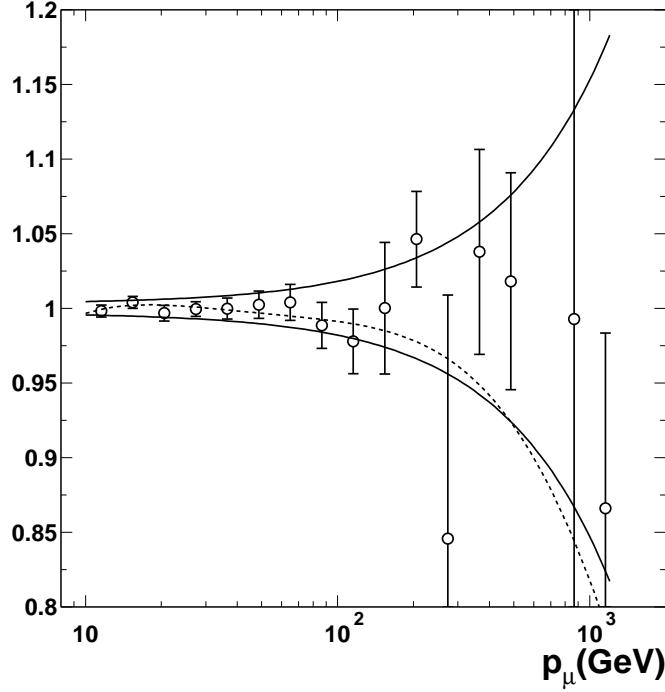


Figure 7: The ratio between the normalized flux data and the fitted function. The band indicates the uncertainty of the fit. The dashed curve represents the normalized reference shape [11].

Figure 7 contains a 1σ error band, which can be approximated by

$$\delta = 0.003 + 0.00015 \cdot \frac{p}{\text{GeV}} \quad (11)$$

It represents the size of the combined relative experimental uncertainties as a function of momentum bin.

The shape uncertainty at reference momenta of 10, 100 and 1000 GeV are 0.5%, 1.8% and 15% respectively. Above 200 GeV the uncertainty rapidly increases, indicating that more measurements are needed at these momenta.

4.2 The absolute normalization of the muon spectrum

In section 4.1 we fitted a functional shape to all renormalized datasets. The renormalization was such that the integral flux above 10 GeV corresponds to the calculation by Bugaev. We will now fit the functional shape obtained in 4.1 to the datasets of those experiments providing an absolute flux measurement, while leaving the normalization as a free parameter. Therefore we fit the function

$$F(p) = C \cdot 10^{H(y)} \quad (12)$$

Data set	χ^2/NDF	Fitted Normalization C
Allkofer 1971 [20]	117/8	1.043 ± 0.006
Ayre 1975 [23]	286/44	0.964 ± 0.002
Bateman 1971 [21]	8/8	0.860 ± 0.008
Green 1979 [24]	2.4/4	0.967 ± 0.022
Tsuji 1998 [26]	16/13	0.948 ± 0.014
De Pascale 1993 [6]	7/5	0.787 ± 0.015
Kremer 1994 data [27]	9/6	0.811 ± 0.009
Kremer 1997 data [27]	11/6	0.820 ± 0.008

Table 3: Normalization factor C with respect to the integrated flux as calculated by Bugaev

The result is shown in table 3. We again ignore the datasets with a very high χ^2/NDF (Allkofer, Ayre). The three remaining data sets with the largest normalization factors (Bateman, Green and Tsuji) are measurements performed with solid iron magnet spectrometers, whereas the other three (Kremer 1994 and 1997 and De Pascale) use the same superconducting magnet. We will first average the normalizations performed by the same collaboration (Bateman and Green, Kremer), and afterwards calculate the normalization measurements performed by the solid iron magnet spectrometers and the superconducting magnet spectrometers, which gives the following results:

$$\begin{array}{l|l} \text{Solid iron magnets} & 0.937 \pm 0.012 \\ \text{Superconducting magnet} & 0.811 \pm 0.007 \end{array}$$

These values are clearly not in agreement. We have no explanation for this observation. We will simply take the average of these two values to be our normalization and half the difference to be the uncertainty. We arrive to our final value of 0.874 ± 0.063 , thus a normalization with a relative uncertainty of 7 %.

4.3 The muon spectrum

In the preceding sections we have parameterized the muon spectrum at sea-level. We summarize the parameters obtained:

$$\begin{array}{ccccc} C & H_1 & H_2 & H_3 & S_2 \\ \hline 0.874 \pm 0.063 & 0.135 \pm 0.002 & -2.529 \pm 0.004 & -5.76 \pm 0.03 & -2.10 \pm 0.03 \end{array}$$

Our description, as well as the calculation from Bugaev, and the measurements used for the normalization are shown in figure 8. The error is given by the estimated normalization uncertainty of 7% and the shape error in (11), added in quadrature.

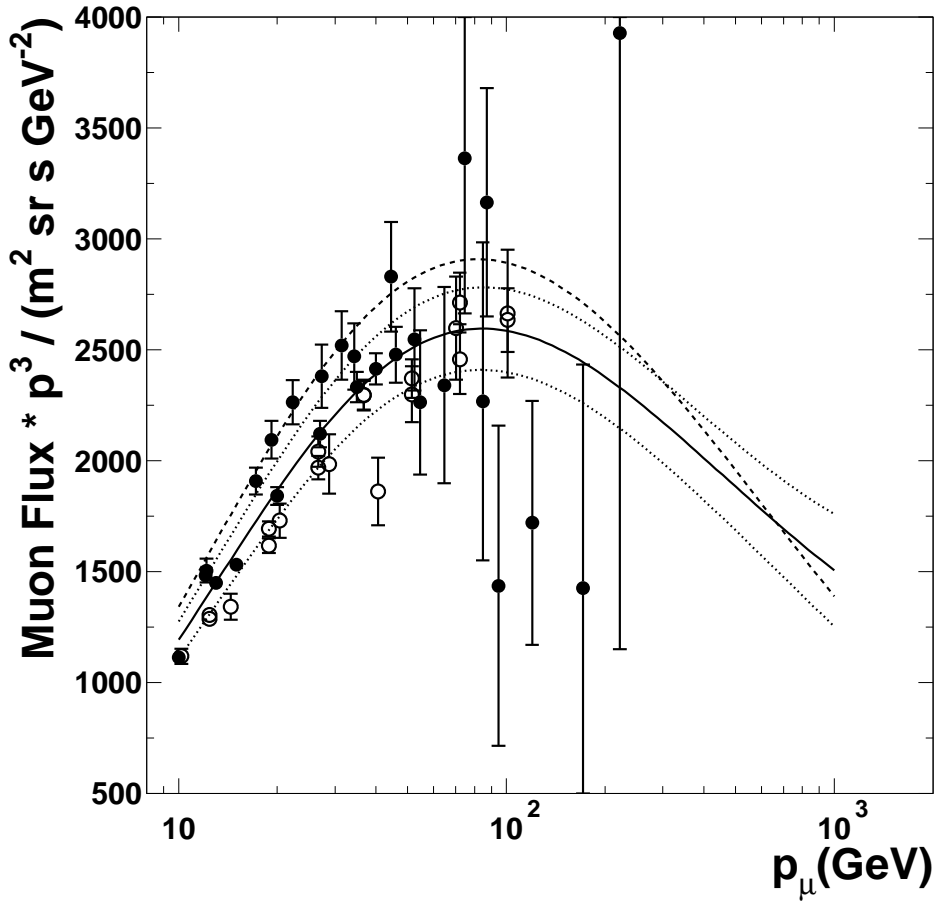


Figure 8: The result on the muon flux. The dotted lines show the 1 sigma error band, whereas the dashed curve is the description by Bugaev. The points are the data used in the normalization procedure. The open points stand for experiments using a superconducting magnet, the black points indicate conventional magnets.

If we compare our description of the differential flux to the theoretical description of Bugaev [11] we get the following :

Momentum:	10 GeV	100 GeV	1000 GeV	
Our Result	1.19 ± 0.08	$(2.59 \pm 0.19) \cdot 10^{-3}$	$(1.52 \pm 0.26) \cdot 10^{-6}$	$\text{m}^{-2} \text{sr}^{-1} \text{s}^{-1} \text{GeV}^{-1}$
Bugaev et al.	1.34	$2.89 \cdot 10^{-3}$	$1.39 \cdot 10^{-6}$	$\text{m}^{-2} \text{sr}^{-1} \text{s}^{-1} \text{GeV}^{-1}$

At 10 GeV the measured flux is 89% of the calculation of Bugaev. However, the measured shape is slightly less steep, and at 1 TeV we arrive to a value which is close to the predicted one.

5. Charge Ratio

The charge ratio R_μ is defined as the ratio of vertical fluxes for positive and negative muons at sea level.

The measured charge ratios together with the published uncertainties are listed in appendix C. Figure 9 shows all values as a function of momentum.

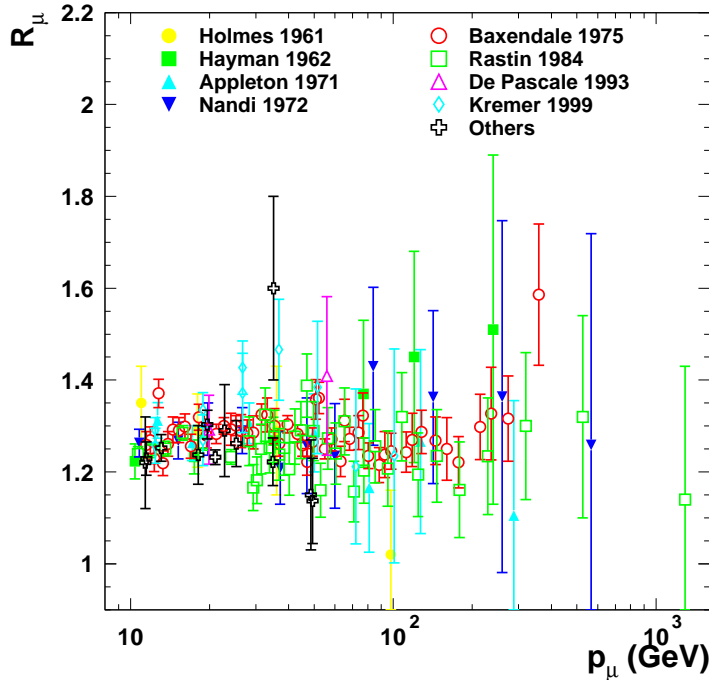


Figure 9: Measured charge ratios.

In order to study the momentum dependence we have grouped all 15 data sets into momentum bins chosen to be equidistant in $\log p$. We have combined the different measurements by assuming that they are uncorrelated. The bin size is relatively large, since a strong momentum dependence is not expected. The result is shown in figure 10. The two data points around 500 GeV and the single measurement above 1 TeV have huge uncertainties ($\sim 20\%$) and are therefore not included in the figure.

For all eight momentum bins the χ^2 values are good or at least acceptable; this implies the various experimental data agree among each other.

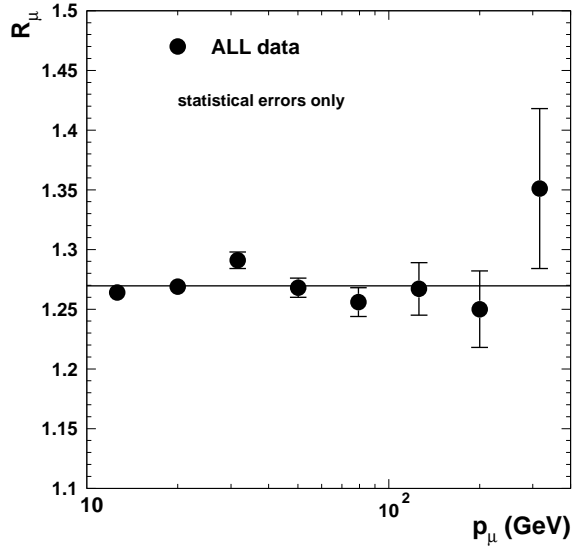


Figure 10: Average charge ratio values.

The third momentum yields the highest charge ratio. However, this result can not be attributed to a single ‘outlier’.

To see if there is a momentum dependence we have performed the following fits to the charge ratio values shown in figure 10 as a function of $\log p$:

a) $f(\log p) = R_\mu^0 = \text{const}$

This gives a good fit with $\chi^2/NDF = 158/142$. The resulting charge ratio of

$$R_\mu^0 = 1.270 \pm 0.003 \quad (13)$$

is displayed in figure 10 as horizontal line.

b) $f(\log p) = R_\mu^1 + S_\mu^1 \cdot \log(p/\text{GeV})$

Naturally this fit is satisfactory, too. The slope comes out as

$$S_\mu^1 = 0.006 \pm 0.011 \quad (14)$$

which is compatible with zero.

Therefore, the measured charge ratios are consistent with the hypothesis of being momentum independent in the range $10 \text{ GeV} \leq p \leq 300 \text{ GeV}$.

We have looked at the data in more detail and tried to answer the following questions:

- i) Do the different experiments agree with each other ?
- ii) Is the ‘peak’ at about 30 GeV significant ?

The previous statistical analyses and figure 9 seem to imply the answer ‘yes’ to the first question. However, when separately plotting the two (by far) most precise data sets (Baxendale 1975[30] and Rastin 1984[31]), one finds the discrepancy displayed in figure 11. Averaged over all momenta the mean values

$$R_\mu^0(\text{Baxendale}) = 1.2799 \pm 0.0042 \quad (15)$$

$$R_\mu^0(\text{Rastin}) = 1.2511 \pm 0.0058 \quad (16)$$

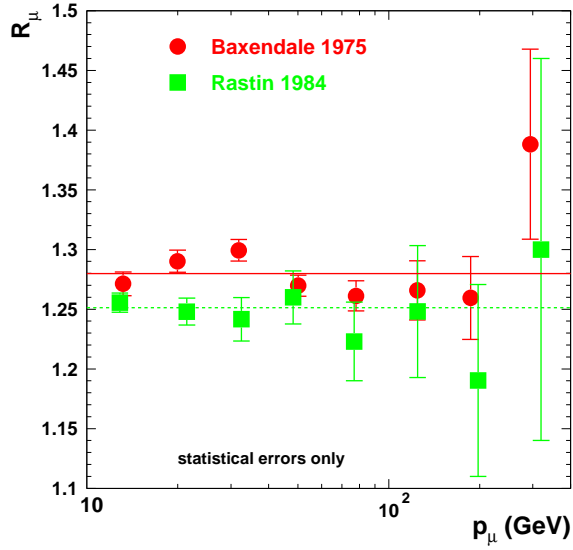


Figure 11: Comparison of charge ratios as measured by Baxendale et al.[30] and Rastin et al.[31].

$\log p/\text{GeV}$	p/GeV	R_μ
1.0-1.2	12.6	1.264 ± 0.009
1.2-1.4	20.0	1.264 ± 0.009
1.4-1.6	31.6	1.283 ± 0.011
1.6-1.8	50.1	1.265 ± 0.014
1.8-2.0	79.4	1.252 ± 0.017
2.0-2.2	126	1.269 ± 0.026
2.2-2.4	200	1.251 ± 0.034
2.4-2.6	316	1.350 ± 0.068

Table 4: Average charge ratios

disagree on the 4σ level. To reduce the discrepancy to about 1σ we assume - in the spirit of the Particle Data Group[32] - that for *all* experiments an additional systematic error of ± 0.015 must be added, in form of a scale uncertainty common to all measurements of one experiment, independent of momentum. Clearly, this is a crude model!

Including these errors results in the charge ratios displayed in figure 12. Note that the values are quite close to those in figure 10, while the error bars are enlarged. The corresponding numbers are listed in table 4. The momenta are calculated from the central values of the logarithmic bins.

There is no final answer to question ii). While the measurements by Baxendale (and also others, with larger errors) indicate an increase of the charge ratio at momenta around 30 GeV, the data by Rastin do not support this hypothesis. For the moment the measurements are consistent with the simple hypothesis of a momentum independent charge ratio.

We try to summarize the charge ratio measurements and their uncertainty (68% CL) with the

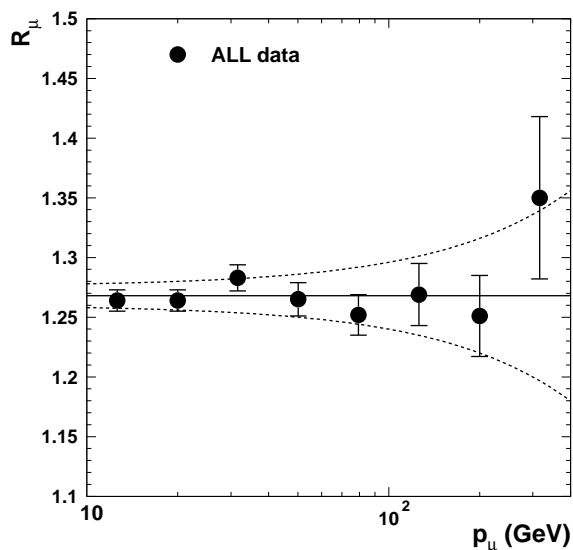


Figure 12: Summary of measured charge ratios and a parameterisation of the central value and the uncertainties.

following formula:

$$R_\mu = 1.268 \pm \left[0.008 + 0.0002 \cdot \frac{p}{\text{GeV}} \right] \quad (17)$$

in the momentum range 10 – 300 GeV. Figure 12 shows the corresponding mean value and the error band. The central value is the mean of all measurements, taking into account the additional systematic error of 0.015. The momentum dependent error is estimated such that it is roughly of the same size as the uncertainties of the corresponding data points in figure 12 and table 4.

Theoretical models of atmospheric showers must be able to reproduce these data, the calculated charge ratios should fall into the band given in equation (17) and figure 12. Clearly, at high momenta precise data is still lacking. Momenta above a few hundred GeV are of particular interest, since a growing influence of kaons and a resulting increase of the charge ratio is predicted[33].

6. Summary and conclusions

We have combined the published data on the vertical muon spectrum and charge ratio at sea-level. In this comparison we have found that the differential spectrum can be described using a simple formula. The shape of the momentum spectrum is well measured at momenta below 100 GeV. Above 200 GeV only a few data points exist, therefore the uncertainty increases to 17 % at 1 TeV.

Several experiments measure the absolute normalization of the spectrum. Our combined result is compared to the calculation by Bugaev et al. At 10 GeV the measured flux is 11 % below the calculated one.

The charge ratio is reported by many experiments. The combined result favors a momentum independent value of the charge ratio of 1.268. The error on the charge ratio increases rapidly above 200 GeV due to a lack of precise experimental data in that region.

7. Acknowledgments

We thank Dieter Heck for helping us to run CORSIKA and Albert van Mil for collecting charge ratio data from the literature.

References

- [1] B. Vulpescu et al, NIM A 414 (1998) 205.
- [2] Super-Kamiokande Collaboration, Y. Fukuda et al, *Phys. Rev. Lett.* **81** (1998) 1562.
- [3] M. Honda et al, Phys. Rev. D 52 (1995) 4985.
- [4] K. Nagashima et al, Nuovo Cim. 12 C (1989) 173.
- [5] D. Heck et al, Report FZKA 6019 (1998), Forschungszentrum Karlsruhe
D. Heck and J. Knapp, Report FZKA 6097 (1998), Forschungszentrum Karlsruhe.
We used CORSIKA version 5.62.
- [6] M.P. De Pascale et al, J. Geoph. Res. 98 (1993) 3501.
- [7] M. Boezio et al., Phys. Rev. D 62 (2000) 032007.
- [8] P.H. Barrett et al, Phys. Rev. 95 (1954) 1573.
- [9] MACRO Collaboration, M. Ambrosio et al, Astropart. Phys. 7 (1997) 109.
- [10] P.J. Hayman and A.W. Wolfendale, Nature 195 (1962) 166.
- [11] E.V. Bugaev et al., Phys. Rev. D 58 (1998) 05401.
- [12] D.E. Caro, J.K. Parry and H.D. Rathgeber, Nature 165 (1950) 689.
- [13] B.G. Owen and J.G. Wilson, Proc. Phys. Soc. (London) A 68 (1955) 409.
- [14] J. Pine, R.J. Davisson and K. Greisen, Nuovo Cim. 14 (1959) 1181.
- [15] W. Pak et al., Phys. Rev. 121 (1961) 905.
- [16] J.E.R. Holmes, B.G. Owen and A.L. Rodgers, Proc. Phys. Soc. (London) 78 (1961) 505.
- [17] P.J. Hayman and A.W. Wolfendale, Proc. Phys. Soc. (London) 80 (1962) 710.
- [18] A.M. Aurela and A.W. Wolfendale, Ann. Acad. Sci. Fenn. A 6 vol 227 (1967) 1.
- [19] I.C. Appleton, M.T. Hogue and B.C. Rastin, Nucl. Phys. B 26 (1971) 365.
- [20] O.C. Allkofer, K. Carstensen and W.D. Dau, Phys. Lett. B 36 (1971) 425.
- [21] B.J. Bateman et al, Phys. Lett. B 36 (1971) 144.
- [22] B.C. Nandi and M.S. Sinha, J. Phys. A 5 (1972) 1384.
- [23] C.A. Ayre et al, J. Phys. G 1 (1975) 584.

- [24] P.J. Green et al, Phys. Rev. D 20 (1979) 1598.
- [25] B.C. Rastin, J. Phys. G 10 (1984) 1609.
- [26] S. Tsuji et al., J. Phys. G 24 (1998) 1805.
- [27] J. Kremer et al, Phys. Rev. Lett. 83 (1999) 4241.
- [28] B. Rossi, Rev. Mod. Phys. 20 (1948) 537.
- [29] B.C. Nandi and M.S. Sinha, Nucl. Phys. B 40 (1972) 289.
- [30] J.M. Baxendale, C.J. Hume and M.G. Thompson, J. Phys. G 1 (1975) 781.
- [31] B.C. Rastin, J. Phys. G 10 (1984) 1629.
- [32] D.E. Groom et al., Eur. Phys. J. C 15 (2000) 1.
- [33] T.K. Gaisser, Cosmic rays and particle physics, Cambridge University Press, 1990.
- [34] B.G. Owen and J.G. Wilson, Proc. Phys. Soc. (London) A 64 (1951) 417.
- [35] B.G. Owen and J.G. Wilson, Proc. Phys. Soc. (London) A 62 (1949) 601.
- [36] I. Filosofo et al, Nuovo Cim. 12 (1954) 809.
- [37] O.C. Allkofer, R.D. Andresen and W.D. Dau, Can. J. Phys. 46 (1968) S301.
- [38] S.R. Baber, W.F. Nash and B.C. Rastin, Nucl. Phys. B 4 (1968) 539.
- [39] S.R. Baber, W.F. Nash and B.C. Rastin, Nucl. Phys. B 4 (1968) 549.
- [40] O.C. Allkofer and W.D. Dau, Phys. Lett. B 38 (1972) 439.

APPENDIX A Measurements.

The following three tables list the experiments/publications we considered, in chronological order, together with the most important parameters.

Some entries are missing since the corresponding figures are not published. In particular the zenith angle regime is characterized frequently only by verbal expressions like ‘near vertical’. We distinguish three magnet types: solid *iron* and conventional coil, *air* gap magnet with conventional coil and air gap magnet with *superconducting* coil. The period of data taking is indicated by year and month, e.g. 59/11 stands for November 1959.

The following remarks refer to the experiment numbers in column 1 of the tables. The figures mentioned are those of the corresponding publication.

- 1) Not used, since data set is a subset of 3)[34].
- 2) Spectrum data read off from figure 1; charge ratio taken from 3)[34].
- 6) Spectrum normalized to Rossi[28]; data read off from figures 8 and 15.
- 7) Spectrum normalized to Rossi.
- 8) Spectrum normalized to Rossi; data read off from figures 1 and 3.
- 9) The two values at $p = 240$ GeV are not statistically independent. We have calculated the arithmetic mean of the two figures and took the smaller of the two statistical errors as the uncertainty.
- 10) We do not use these data, which were obtained in the equator region, where the geomagnetic cutoff is large (14 GeV) and may influence the muon flux.
- 11) The spectrum data form a subset of those published in 13)[19]. Nevertheless we consider it separately, since the normalization procedures are slightly different. When calculating world averages we exclude these data. We do not use the charge ratio data, since they are included in the superset published in 13)[19].
- 13) Spectrum: no absolute flux determination, only normalization to previous measurements by other experiments. Charge ratio: A few measurements are given with slightly asymmetric errors; they have been ‘symmetrized’ by shifting the central value to the center of the error interval.
- 15) Apparatus under concrete shelter of 868 g/cm^2 .
- 16) We use only the charge ratio value obtained at the town of Kiel[20]; for the other measurements, made at muon momenta close to and below 10 GeV in the equator region, the geomagnetic cutoff is large (14 GeV) and may influence the muon flux.
- 20) Resolution correction is based upon $\text{MDM} = 100$ GeV; if MDM of 350 GeV is used, spectrum is flatter and better consistent with 18) [23]. Points up to 100 GeV are considered reliable.
- 21) Spectrum data are normalized to an integral intensity at 5 GeV. The spectrum provided is the theoretical spectrum that fits the data best.
- 22) Above 50 GeV authors question results due to resolution.
- 24, 25) Same magnet as 22)[6]. Charge ratio and its error read off from figure 2.

No	author(s), reference	name	location	coordinates	alt. /m	magnet	detector(s)	period	MDM /GeV	zenith	spec.	ratio
1	B.G. Owen and J.G. Wilson, 1949[35]		Manchester (Great Britain)	53 ⁰ N, 2 ⁰ W	50	air	Geiger, flash tubes		30	< 8 ⁰	no	yes
2	D.E. Caro et al, 1950[12]		Melbourne (Australia)	38 ⁰ S, 145 ⁰ E	50	air	counters		≈ 50		yes	yes
3	B.G. Owen and J.G. Wilson, 1951[34]		Manchester (Great Britain)	53 ⁰ N, 2 ⁰ W	50	air	Geiger, flash tubes		30	< 8 ⁰	no	yes
4	I. Filosofo et. al, 1954[36]		Agordo (Italy)	46 ⁰ N, 12 ⁰ E	600	iron	counters				no	yes
5	B.G. Owen and J.G. Wilson, 1955[13]		Manchester (Great Britain)	53 ⁰ N, 2 ⁰ W	50	air	counters			< 10 ⁰	yes	no
6	J. Pine et al, 1959[14]		Cornell (USA)	42 ⁰ N, 76 ⁰ W	500	air	Geiger, cloud ch.		175		yes	yes
7	J.E.R. Holmes et al, 1961[16]		Manchester (Great Britain)	53 ⁰ N, 2 ⁰ W	50	air	cloud ch., Geiger	53-55		< 10 ⁰	yes	yes
8	W. Pak et al, 1961[15]		Cornell (USA)	42 ⁰ N, 76 ⁰ W	500	air	Geiger, hodosc.		175		yes	yes
9	P.J. Hayman and A.W. Wolfendale, 1962[17, 10]		Durham (Great Britain)	54 ⁰ N, 1 ⁰ W	70	air	Geiger, flash tubes	59/11-60/03	657		yes	yes
10	O.C. Allkofer et al, 1968[37]		near equator	29 ⁰ W, 0 ⁰ N 22 ⁰ W, 1 ⁰ S	0	air	spark ch.				yes	yes

No	author(s), reference	name	location	coordinates	alt. /m	magnet	detector(s)	period	MDM /GeV	zenith	spec.	ratio
11	S.R. Baber et al, 1968[38, 39]		Nottingham (Great Britain)	53 ⁰ N, 1 ⁰ W	52	iron	Geiger	64/06-65/05	360		yes	yes
12	A.M. Aurela and A.W. Wolfendale, 1967[18]		Durham (Great Britain)	54 ⁰ N, 1 ⁰ W	70	air, iron	Geiger, flash	64/06-65/01			yes	no
13	I.C. Appleton et al, 1971[19]		Nottingham (Great Britain)	53 ⁰ N, 1 ⁰ W	52	iron	flash tubes	64-68	360		yes	yes
14	B.J. Bateman et al, 1971[21]	AMH	College Station (USA)	31 ⁰ N, 96 ⁰ W	80	iron	spark ch., scint.				yes	no
15	O.C. Allkofer et al, 1971[20]		Kiel (Germany)	54 ⁰ N, 11 ⁰ E	10	iron	spark ch., scint.		> 1000		yes	no
16	O.C. Allkofer and W.D. Dau, 1972[40]		Kiel (and equator)	54 ⁰ N, 11 ⁰ E	10	iron	spark ch., scint.				no	yes
17	B.C. Nandi et al, 1972[29, 22]		Durgapur (India)	24 ⁰ N, 87 ⁰ E	70	iron	flash tubes, Geiger	69/02-70/02	985		yes	yes
18	C.A. Ayre et al, 1975[23]	MARS	Durham (Great Britain)	54 ⁰ N, 1 ⁰ W	70	iron	scint., flash tubes	72/05-73/01	670		yes	no
19	J.M. Baxendale et al, 1975[30]		Durham (Great Britain)	54 ⁰ N, 1 ⁰ W	70	iron	scint., flash tubes	72/02-72/12			yes	yes
20	P.J. Green et al, 1979[24]	AMH	Houston (USA)	30 ⁰ N, 95 ⁰ W	10	iron	spark ch., scint.		345	< 9 ⁰	yes	no

No	author(s), reference	name	location	coordinates	alt. /m	magnet	detector(s)	period	MDM /GeV	zenith	spec.	ratio
21	B.C. Rastin 1984[25, 31]		Nottingham (Great Britain)	53 ⁰ N, 1 ⁰ W	52	iron	flash tubes, scint.	74/09-78/05	3400		yes	yes
22	M.P. De Pascale et al, 1993[6]	MASS	Prince Albert (Canada)	53 ⁰ N, 106 ⁰ W	600	air (superc.)	MWPC, scint., TOF	89/08	118		yes	yes
23	S. Tsuji et al, 1998[26]		Okayama (Japan)	34 ⁰ N, 134 ⁰ E	5	iron	drift, scint.	92/09-97/12	270	0 ⁰ -1 ⁰	yes	no
24	J. Kremer et al, 1999[27]	CAPRICE	Lynn Lake (Canada)	57 ⁰ N, 101 ⁰ W	360	air (superc.)	prop., drift, TOF, RICH	94/07	175	0 ⁰ -20 ⁰	yes	yes
25	J. Kremer et al, 1999[27]	CAPRICE	Fort Sumner (USA)	34 ⁰ N, 104 ⁰ W	1270	air (superc.)	drift, TOF, RICH	97/04-97/05	175	0 ⁰ -20 ⁰	yes	yes

APPENDIX B Muon flux data.

The following lists contain all spectrum data for momenta above 10 GeV. The flux is given in ($\text{m}^{-2} \text{sr}^{-1} \text{s}^{-1} \text{GeV}$). Each line contains the momentum in GeV together with the published value and uncertainty of the flux. Altitude corrections have been applied later and are not included in the figures listed here.

- D.E. Caro et al, 1950[12]

12.2	$(6.46 \pm 0.75) \cdot 10^{-1}$
16.9	$(2.59 \pm 0.26) \cdot 10^{-1}$
17.8	$(2.38 \pm 0.25) \cdot 10^{-1}$
26.5	$(7.4 \pm 0.9) \cdot 10^{-2}$
51	$(1.3 \pm 0.2) \cdot 10^{-2}$

- B.G. Owen and J.G. Wilson, 1955[13]

10.0	1.09 ± 0.03
15.0	$(4.36 \pm 0.11) \cdot 10^{-1}$
20.0	$(2.20 \pm 0.06) \cdot 10^{-1}$

- J.Pine et al, 1959[14]

11.6	$(8.26 \pm 0.99) \cdot 10^{-1}$
13.7	$(5.24 \pm 0.84) \cdot 10^{-1}$
16.3	$(3.05 \pm 0.49) \cdot 10^{-1}$
18.1	$(2.79 \pm 0.33) \cdot 10^{-1}$
19.8	$(1.91 \pm 0.31) \cdot 10^{-1}$
25.5	$(1.16 \pm 0.19) \cdot 10^{-1}$
29.8	$(7.68 \pm 0.92) \cdot 10^{-2}$
35.4	$(4.95 \pm 0.79) \cdot 10^{-2}$
46.0	$(1.99 \pm 0.32) \cdot 10^{-2}$
59.1	$(9.29 \pm 1.49) \cdot 10^{-3}$
83.2	$(4.60 \pm 0.87) \cdot 10^{-3}$
125.	$(1.34 \pm 0.33) \cdot 10^{-3}$

- W.Pak et al, 1961[15]

12.9	$(6.14 \pm 0.68) \cdot 10^{-1}$
15.8	$(3.35 \pm 0.37) \cdot 10^{-1}$
19.8	$(1.89 \pm 0.21) \cdot 10^{-1}$
24.1	$(1.35 \pm 0.19) \cdot 10^{-1}$
26.4	$(1.03 \pm 0.11) \cdot 10^{-1}$
37.4	$(3.77 \pm 0.41) \cdot 10^{-2}$
58.9	$(1.29 \pm 0.14) \cdot 10^{-2}$

- J.E.R. Holmes et al, 1961[16]

11	$(7.88 \pm 0.32) \cdot 10^{-1}$
13	$(5.90 \pm 0.30) \cdot 10^{-1}$
16	$(3.68 \pm 0.18) \cdot 10^{-1}$
19	$(2.33 \pm 0.12) \cdot 10^{-1}$
23	$(1.67 \pm 0.12) \cdot 10^{-1}$
28	$(1.04 \pm 0.07) \cdot 10^{-1}$
36	$(5.75 \pm 0.40) \cdot 10^{-2}$
49	$(2.02 \pm 0.20) \cdot 10^{-2}$
67	$(8.65 \pm 1.30) \cdot 10^{-3}$
89	$(4.38 \pm 0.70) \cdot 10^{-3}$
134	$(1.42 \pm 0.26) \cdot 10^{-3}$
271	$(2.8 \pm 0.6) \cdot 10^{-4}$
1160	$(4.8 \pm 2.3) \cdot 10^{-6}$

- P.J. Hayman and A.W. Wolfendale 1962[17]

10.8	$(8.51 \pm 0.26) \cdot 10^{-1}$
12.4	$(6.14 \pm 0.17) \cdot 10^{-1}$
14.6	$(4.35 \pm 0.11) \cdot 10^{-1}$
17.8	$(2.52 \pm 0.07) \cdot 10^{-1}$
22.6	$(1.39 \pm 0.04) \cdot 10^{-1}$
31.3	$(5.85 \pm 0.15) \cdot 10^{-2}$
42.3	$(2.88 \pm 0.11) \cdot 10^{-2}$
56.1	$(1.22 \pm 0.05) \cdot 10^{-2}$
72.5	$(5.75 \pm 0.46) \cdot 10^{-3}$
88.1	$(3.27 \pm 0.29) \cdot 10^{-3}$
112	$(1.36 \pm 0.14) \cdot 10^{-3}$
153	$(5.18 \pm 0.93) \cdot 10^{-4}$
244	$(1.14 \pm 0.22) \cdot 10^{-4}$
413	$(1.98 \pm 0.99) \cdot 10^{-5}$
894	$(1.84 \pm 1.01) \cdot 10^{-6}$

- A.M. Aurela and A.W. Wolfendale 1967[18]

15.1	$(4.25 \pm 0.16) \cdot 10^{-1}$
41.5	$(3.40 \pm 0.44) \cdot 10^{-2}$
82.1	$(4.10 \pm 0.35) \cdot 10^{-3}$

- S.R. Baber et al, 1968[38]

11.60	$(7.77 \pm 0.26) \cdot 10^{-1}$
15.22	$(4.22 \pm 0.21) \cdot 10^{-1}$
19.20	$(2.42 \pm 0.12) \cdot 10^{-1}$
24.00	$(1.39 \pm 0.07) \cdot 10^{-1}$
33.5	$(5.78 \pm 0.35) \cdot 10^{-2}$
50.0	$(1.90 \pm 0.16) \cdot 10^{-2}$
81.0	$(4.59 \pm 0.60) \cdot 10^{-3}$
127.0	$(1.14 \pm 0.18) \cdot 10^{-3}$
266.0	$(1.00 \pm 0.24) \cdot 10^{-4}$
810.0	$(2.11 \pm 0.55) \cdot 10^{-6}$

- I.C. Appleton et al, 1971[19]

12.84	$(2.92 \pm 0.04) \cdot 10^{-1}$
17.2	$(1.46 \pm 0.02) \cdot 10^{-1}$
24.3	$(5.78 \pm 0.13) \cdot 10^{-2}$
33	$(2.54 \pm 0.06) \cdot 10^{-2}$
43.4	$(1.09 \pm 0.10) \cdot 10^{-2}$
45.6	$(1.07 \pm 0.09) \cdot 10^{-2}$
48.2	$(9.00 \pm 0.81) \cdot 10^{-3}$
51.0	$(6.95 \pm 0.67) \cdot 10^{-3}$
54.2	$(6.84 \pm 0.63) \cdot 10^{-3}$
57.9	$(5.20 \pm 0.52) \cdot 10^{-3}$
62.0	$(4.79 \pm 0.47) \cdot 10^{-3}$
66.9	$(2.80 \pm 0.33) \cdot 10^{-3}$
72.6	$(2.76 \pm 0.31) \cdot 10^{-3}$
79.3	$(2.02 \pm 0.23) \cdot 10^{-3}$
87.5	$(1.57 \pm 0.17) \cdot 10^{-3}$
97.6	$(1.17 \pm 0.13) \cdot 10^{-3}$
110.3	$(6.97 \pm 0.94) \cdot 10^{-4}$
129.9	$(3.00 \pm 0.54) \cdot 10^{-4}$
149.4	$(2.93 \pm 0.29) \cdot 10^{-4}$
181.5	$(1.34 \pm 0.24) \cdot 10^{-4}$
230.9	$(6.61 \pm 1.41) \cdot 10^{-5}$
316.1	$(2.72 \pm 0.59) \cdot 10^{-5}$
491.5	$(7.67 \pm 1.69) \cdot 10^{-6}$
1000.0	$(5.21 \pm 1.34) \cdot 10^{-7}$

- B.J. Bateman et al, 1971[21]

10.0	1.12 ± 0.03
13.0	$(6.63 \pm 0.13) \cdot 10^{-1}$
15.0	$(4.56 \pm 0.09) \cdot 10^{-1}$
20.0	$(2.31 \pm 0.05) \cdot 10^{-1}$
27.0	$(1.08 \pm 0.03) \cdot 10^{-1}$
35.0	$(5.45 \pm 0.16) \cdot 10^{-2}$
40.0	$(3.78 \pm 0.11) \cdot 10^{-2}$
46.0	$(2.55 \pm 0.13) \cdot 10^{-2}$
53.0	$(1.70 \pm 0.08) \cdot 10^{-2}$

- O.C. Allkofer et al, 1971[20]

11.4	1.13 ± 0.01
14.8	$(6.04 \pm 0.08) \cdot 10^{-1}$
20.5	$(2.51 \pm 0.03) \cdot 10^{-1}$
31.4	$(8.01 \pm 0.13) \cdot 10^{-2}$
52.3	$(1.89 \pm 0.05) \cdot 10^{-2}$
93.0	$(3.38 \pm 0.14) \cdot 10^{-3}$
175.0	$(5.19 \pm 0.37) \cdot 10^{-4}$
329.0	$(7.84 \pm 1.12) \cdot 10^{-5}$
642.0	$(6.40 \pm 1.92) \cdot 10^{-6}$

- B.C. Nandi and M.S. Sinha, 1972[22]

11.8	$(9.43 \pm 0.15) \cdot 10^{-1}$
14.0	$(6.38 \pm 0.14) \cdot 10^{-1}$
16.4	$(4.21 \pm 0.09) \cdot 10^{-1}$
19.7	$(2.72 \pm 0.06) \cdot 10^{-1}$
24.2	$(1.41 \pm 0.04) \cdot 10^{-1}$
29.6	$(1.01 \pm 0.03) \cdot 10^{-1}$
37.1	$(5.40 \pm 0.17) \cdot 10^{-2}$
46.9	$(2.99 \pm 0.13) \cdot 10^{-2}$
60.0	$(1.45 \pm 0.07) \cdot 10^{-2}$
84.0	$(5.58 \pm 0.28) \cdot 10^{-3}$
118	$(2.04 \pm 0.17) \cdot 10^{-3}$
167	$(6.09 \pm 0.61) \cdot 10^{-4}$
260	$(1.96 \pm 0.25) \cdot 10^{-4}$
467	$(2.69 \pm 0.67) \cdot 10^{-5}$
1109	$(1.03 \pm 0.36) \cdot 10^{-6}$

- C.A. Ayre et al, 1975[23]

21.3	$(2.096 \pm 0.029) \cdot 10^{-1}$
22.1	$(1.909 \pm 0.027) \cdot 10^{-1}$
23.1	$(1.708 \pm 0.024) \cdot 10^{-1}$
24.1	$(1.574 \pm 0.022) \cdot 10^{-1}$
25.1	$(1.432 \pm 0.020) \cdot 10^{-1}$
26.3	$(1.224 \pm 0.017) \cdot 10^{-1}$
27.7	$(1.067 \pm 0.015) \cdot 10^{-1}$
29.3	$(9.130 \pm 0.128) \cdot 10^{-2}$
31.0	$(7.968 \pm 0.112) \cdot 10^{-2}$
33.1	$(6.947 \pm 0.097) \cdot 10^{-2}$
35.3	$(5.704 \pm 0.080) \cdot 10^{-2}$
38.3	$(4.547 \pm 0.068) \cdot 10^{-2}$
40.8	$(4.208 \pm 0.046) \cdot 10^{-2}$
41.7	$(3.663 \pm 0.055) \cdot 10^{-2}$
42.8	$(3.420 \pm 0.041) \cdot 10^{-2}$
44.8	$(2.962 \pm 0.036) \cdot 10^{-2}$
45.8	$(2.797 \pm 0.042) \cdot 10^{-2}$
47.1	$(2.628 \pm 0.032) \cdot 10^{-2}$
49.3	$(2.217 \pm 0.027) \cdot 10^{-2}$
50.7	$(2.086 \pm 0.033) \cdot 10^{-2}$
52.1	$(2.014 \pm 0.024) \cdot 10^{-2}$
55.2	$(1.646 \pm 0.021) \cdot 10^{-2}$
57.0	$(1.525 \pm 0.024) \cdot 10^{-2}$
58.9	$(1.434 \pm 0.019) \cdot 10^{-2}$
63.0	$(1.123 \pm 0.015) \cdot 10^{-2}$
65.3	$(1.023 \pm 0.017) \cdot 10^{-2}$
67.9	$(9.216 \pm 0.129) \cdot 10^{-3}$
73.7	$(7.084 \pm 0.099) \cdot 10^{-3}$
76.6	$(6.585 \pm 0.118) \cdot 10^{-3}$
80.0	$(5.753 \pm 0.081) \cdot 10^{-3}$
88.3	$(4.149 \pm 0.062) \cdot 10^{-3}$
93.0	$(3.616 \pm 0.072) \cdot 10^{-3}$
98.3	$(3.252 \pm 0.052) \cdot 10^{-3}$
112.0	$(2.037 \pm 0.035) \cdot 10^{-3}$
118.0	$(1.842 \pm 0.042) \cdot 10^{-3}$
128.0	$(1.454 \pm 0.026) \cdot 10^{-3}$
145.0	$(9.603 \pm 0.192) \cdot 10^{-4}$
160.0	$(7.459 \pm 0.201) \cdot 10^{-4}$
177.0	$(5.352 \pm 0.123) \cdot 10^{-4}$
214.0	$(2.893 \pm 0.078) \cdot 10^{-4}$
236.0	$(2.171 \pm 0.083) \cdot 10^{-4}$
274.0	$(1.260 \pm 0.044) \cdot 10^{-4}$
358.0	$(5.328 \pm 0.250) \cdot 10^{-5}$
367.0	$(4.843 \pm 0.349) \cdot 10^{-5}$
442.0	$(2.764 \pm 0.221) \cdot 10^{-5}$

- P.J. Green et al, 1979[24]

12.18	$(8.33 \pm 0.30) \cdot 10^{-1}$
19.20	$(2.96 \pm 0.12) \cdot 10^{-1}$
31.40	$(8.14 \pm 0.50) \cdot 10^{-2}$
52.40	$(1.77 \pm 0.16) \cdot 10^{-2}$
87.10	$(4.79 \pm 0.78) \cdot 10^{-3}$
(249.90	$(3.95 \pm 0.53) \cdot 10^{-4}$)

- B.C. Rastin, 1984[31]

10.69	1.156 ± 0.008
11.94	$(9.05 \pm 0.06) \cdot 10^{-1}$
13.58	$(6.72 \pm 0.04) \cdot 10^{-1}$
15.81	$(4.70 \pm 0.03) \cdot 10^{-1}$
19.05	$(2.97 \pm 0.02) \cdot 10^{-1}$
24.14	$(1.63 \pm 0.01) \cdot 10^{-1}$
28.35	$(1.03 \pm 0.02) \cdot 10^{-1}$
29.30	$(9.3 \pm 0.2) \cdot 10^{-2}$
30.32	$(8.5 \pm 0.2) \cdot 10^{-2}$
31.42	$(7.8 \pm 0.2) \cdot 10^{-2}$
32.60	$(7.1 \pm 0.2) \cdot 10^{-2}$
33.88	$(6.3 \pm 0.1) \cdot 10^{-2}$
35.27	$(5.8 \pm 0.1) \cdot 10^{-2}$
36.79	$(5.1 \pm 0.1) \cdot 10^{-2}$
38.44	$(4.4 \pm 0.1) \cdot 10^{-2}$
40.25	$(3.91 \pm 0.09) \cdot 10^{-2}$
42.25	$(3.44 \pm 0.08) \cdot 10^{-2}$
44.47	$(3.03 \pm 0.07) \cdot 10^{-2}$
46.94	$(2.62 \pm 0.06) \cdot 10^{-2}$
49.71	$(2.23 \pm 0.06) \cdot 10^{-2}$
52.84	$(1.87 \pm 0.05) \cdot 10^{-2}$
56.40	$(1.56 \pm 0.04) \cdot 10^{-2}$
60.49	$(1.25 \pm 0.03) \cdot 10^{-2}$
65.23	$(1.04 \pm 0.03) \cdot 10^{-2}$
70.80	$(7.6 \pm 0.2) \cdot 10^{-3}$
77.42	$(6.3 \pm 0.2) \cdot 10^{-3}$
85.43	$(4.4 \pm 0.1) \cdot 10^{-3}$
95.34	$(3.2 \pm 0.1) \cdot 10^{-3}$
107.88	$(2.12 \pm 0.08) \cdot 10^{-3}$
124.27	$(1.42 \pm 0.05) \cdot 10^{-3}$
146.62	$(8.8 \pm 0.4) \cdot 10^{-4}$
178.85	$(4.8 \pm 0.2) \cdot 10^{-4}$
229.36	$(2.2 \pm 0.1) \cdot 10^{-4}$
319.72	$(7.5 \pm 0.5) \cdot 10^{-5}$
525.82	$(1.4 \pm 0.1) \cdot 10^{-5}$
1288.74	$(5.9 \pm 0.8) \cdot 10^{-7}$

- M.P. De Pascale et al, 1993[6]

Positive Muons:

10.19	$(5.983 \pm 0.233) \cdot 10^{-1}$
14.42	$(2.523 \pm 0.144) \cdot 10^{-1}$
20.36	$(1.246 \pm 0.071) \cdot 10^{-1}$
28.80	$(4.709 \pm 0.414) \cdot 10^{-2}$
40.64	$(1.430 \pm 0.162) \cdot 10^{-2}$
70.16	$(5.176 \pm 0.554) \cdot 10^{-3}$

Negative Muons:

10.19	$(5.025 \pm 0.216) \cdot 10^{-1}$
14.42	$(2.124 \pm 0.132) \cdot 10^{-1}$
20.36	$(8.653 \pm 0.580) \cdot 10^{-2}$
28.80	$(3.788 \pm 0.375) \cdot 10^{-2}$
40.64	$(1.389 \pm 0.158) \cdot 10^{-2}$
70.16	$(2.423 \pm 0.383) \cdot 10^{-3}$

- S. Tsuji et al, 1998[26]

12.1	$(8.37 \pm 0.17) \cdot 10^{-1}$
17.2	$(3.75 \pm 0.12) \cdot 10^{-1}$
22.3	$(2.04 \pm 0.09) \cdot 10^{-1}$
27.3	$(1.17 \pm 0.07) \cdot 10^{-1}$
34.3	$(6.12 \pm 0.37) \cdot 10^{-2}$
44.5	$(3.21 \pm 0.28) \cdot 10^{-2}$
54.6	$(1.39 \pm 0.20) \cdot 10^{-2}$
64.6	$(8.68 \pm 1.64) \cdot 10^{-3}$
74.7	$(8.07 \pm 1.68) \cdot 10^{-3}$
84.7	$(3.73 \pm 1.18) \cdot 10^{-3}$
94.7	$(1.69 \pm 0.85) \cdot 10^{-3}$
119.8	$(1.00 \pm 0.32) \cdot 10^{-3}$
171.2	$(2.84 \pm 2.01) \cdot 10^{-4}$
222.0	$(3.59 \pm 2.54) \cdot 10^{-4}$

- J. Kremer et al, 1999[27] 1994 data

Positive Muons:

12.42	$(3.89 \pm 0.08) \cdot 10^{-1}$
18.85	$(1.38 \pm 0.04) \cdot 10^{-1}$
26.68	$(6.3 \pm 0.3) \cdot 10^{-2}$
36.69	$(2.8 \pm 0.1) \cdot 10^{-2}$
51.47	$(9.9 \pm 0.7) \cdot 10^{-3}$
72.08	$(3.6 \pm 0.3) \cdot 10^{-3}$
100.96	$(1.4 \pm 0.2) \cdot 10^{-3}$

Negative Muons:

12.42	$(3.09 \pm 0.07) \cdot 10^{-1}$
18.85	$(1.08 \pm 0.03) \cdot 10^{-1}$
26.68	$(4.6 \pm 0.2) \cdot 10^{-2}$
36.69	$(1.9 \pm 0.1) \cdot 10^{-2}$
51.47	$(7.1 \pm 0.6) \cdot 10^{-3}$
72.08	$(3.0 \pm 0.3) \cdot 10^{-3}$
100.96	$(1.2 \pm 0.2) \cdot 10^{-3}$

- J. Kremer et al, 1999[27] 1997 data

Positive Muons:

12.42	$(4.14 \pm 0.09) \cdot 10^{-1}$
18.85	$(1.54 \pm 0.04) \cdot 10^{-1}$
26.68	$(6.4 \pm 0.2) \cdot 10^{-2}$
36.69	$(2.8 \pm 0.1) \cdot 10^{-2}$
51.47	$(10.2 \pm 0.5) \cdot 10^{-3}$
72.08	$(4.2 \pm 0.3) \cdot 10^{-3}$
100.96	$(1.5 \pm 0.1) \cdot 10^{-3}$

Negative Muons:

12.42	$(3.20 \pm 0.07) \cdot 10^{-1}$
18.85	$(1.16 \pm 0.03) \cdot 10^{-1}$
26.68	$(4.5 \pm 0.2) \cdot 10^{-2}$
36.69	$(2.03 \pm 0.08) \cdot 10^{-2}$
51.47	$(7.7 \pm 0.4) \cdot 10^{-3}$
72.08	$(3.2 \pm 0.2) \cdot 10^{-3}$
100.96	$(1.1 \pm 0.1) \cdot 10^{-3}$

APPENDIX C Charge ratio data.

The following lists contain all charge ratio data for momenta above 10 GeV. Each line contains the momentum in GeV together with the published value and uncertainty of the charge ratio.

- D.E. Caro et al, 1950[12]

35.0 1.6 ± 0.2

- B.G. Owen et al, 1951[34]

11.5 1.229 ± 0.036

- I. Filosofo et al, 1954[36]

21.0 1.232 ± 0.016

- J. Pine et al, 1959[14]

19.6 1.303 ± 0.031
22.8 1.29 ± 0.10
34.8 1.222 ± 0.052
48.6 1.15 ± 0.12

- J.E.R. Holmes et al, 1961[16]

6.7 1.39 ± 0.08
11.0 1.35 ± 0.08
18.0 1.29 ± 0.08
36.0 1.29 ± 0.14
98.0 1.02 ± 0.14

- W. Pak et al, 1961[15]

13.1 1.252 ± 0.029
18.1 1.237 ± 0.064
25.3 1.262 ± 0.050
49.3 1.137 ± 0.093

- P.J. Hayman and A.W. Wolfendale, 1962[10]

10.4 1.223 ± 0.038
17.5 1.233 ± 0.037
35.0 1.268 ± 0.051
77.0 1.37 ± 0.16
120.0 1.45 ± 0.23
240.0 1.51 ± 0.38

- I.C. Appleton et al, 1971[19]

12.7 1.312 ± 0.039
17.2 1.263 ± 0.038
28.3 1.306 ± 0.044
50.0 1.285 ± 0.085
81.0 1.165 ± 0.14
127.0 1.266 ± 0.20
288.0 1.105 ± 0.25

- O.C. Allkofer and W.D. Dau, 1972[40]

11.4 1.22 ± 0.10

- B.C. Nandi et al, 1972[29]

10.8 1.263 ± 0.030
15.2 1.268 ± 0.040
19.7 1.293 ± 0.057
26.6 1.290 ± 0.050
37.1 1.209 ± 0.079
46.9 1.257 ± 0.104
60.0 1.235 ± 0.114
84.0 1.430 ± 0.172
142.0 1.363 ± 0.188
260.0 1.364 ± 0.383
566.0 1.259 ± 0.460

- J.M. Baxendale et al, 1975[30]

11.5	1.259 ± 0.029
11.9	1.269 ± 0.029
12.3	1.229 ± 0.028
12.8	1.371 ± 0.031
13.3	1.219 ± 0.027
13.9	1.261 ± 0.027
14.5	1.292 ± 0.028
15.3	1.291 ± 0.027
16.1	1.299 ± 0.027
17.0	1.256 ± 0.026
18.2	1.319 ± 0.028
19.5	1.279 ± 0.027
21.2	1.283 ± 0.021
22.7	1.300 ± 0.018
24.1	1.293 ± 0.035
25.2	1.301 ± 0.022
26.3	1.289 ± 0.036
27.8	1.285 ± 0.028
29.3	1.286 ± 0.036
31.5	1.325 ± 0.023
33.1	1.324 ± 0.037
35.3	1.300 ± 0.038
36.8	1.262 ± 0.028
39.6	1.304 ± 0.019
43.2	1.283 ± 0.019
45.2	1.258 ± 0.024
47.1	1.222 ± 0.029
49.3	1.265 ± 0.031
50.7	1.358 ± 0.043
52.1	1.361 ± 0.034
54.9	1.250 ± 0.022
58.2	1.271 ± 0.025
63.0	1.223 ± 0.033
65.3	1.312 ± 0.046
68.1	1.272 ± 0.025
73.7	1.286 ± 0.037
76.6	1.323 ± 0.049
80.4	1.235 ± 0.028
88.3	1.215 ± 0.038
93.0	1.238 ± 0.050
98.3	1.245 ± 0.039
112.0	1.243 ± 0.044
118.0	1.270 ± 0.058
128.0	1.287 ± 0.047
145.0	1.268 ± 0.052

160.0	1.250 ± 0.068
177.0	1.221 ± 0.056
214.0	1.298 ± 0.071
236.0	1.327 ± 0.101
274.0	1.316 ± 0.093
358.0	1.586 ± 0.154

- B.C. Rastin, 1984[31]

10.69	1.239 ± 0.016
11.94	1.247 ± 0.016
13.58	1.251 ± 0.016
15.81	1.285 ± 0.016
19.05	1.263 ± 0.016
24.14	1.233 ± 0.016
28.35	1.267 ± 0.053
29.30	1.166 ± 0.050
30.32	1.182 ± 0.051
31.42	1.250 ± 0.054
32.60	1.325 ± 0.058
33.88	1.253 ± 0.055
35.27	1.277 ± 0.057
36.79	1.238 ± 0.056
38.44	1.252 ± 0.059
40.25	1.206 ± 0.057
42.25	1.277 ± 0.060
44.47	1.291 ± 0.062
46.94	1.388 ± 0.069
49.71	1.289 ± 0.064
52.84	1.160 ± 0.059
56.40	1.273 ± 0.067
60.49	1.240 ± 0.067
65.23	1.310 ± 0.073
70.80	1.157 ± 0.066
77.42	1.203 ± 0.071
85.43	1.256 ± 0.080
95.34	1.207 ± 0.082
107.88	1.320 ± 0.096
124.27	1.194 ± 0.091
146.62	1.235 ± 0.101
178.85	1.161 ± 0.104
229.36	1.234 ± 0.127
319.72	1.30 ± 0.16
525.82	1.32 ± 0.22
1288.74	1.14 ± 0.29

- M.P. De Pascale et al, 1993[6]

19.89 1.292 ± 0.075
55.87 1.409 ± 0.173

- J. Kremer et al, 1999[27] 1994 data

12.42 1.257 ± 0.038
18.85 1.269 ± 0.055
26.68 1.372 ± 0.086
36.69 1.466 ± 0.110
51.47 1.384 ± 0.144
72.08 1.212 ± 0.169
100.96 1.235 ± 0.233

- J. Kremer et al, 1999[27] 1997 data

12.42 1.291 ± 0.027
18.85 1.335 ± 0.038
26.68 1.427 ± 0.058
36.69 1.383 ± 0.068
51.47 1.320 ± 0.090
72.08 1.337 ± 0.120
100.96 1.337 ± 0.169

APPENDIX D Correlation matrix for the fit of the spectrum shape:

	H_3	H_2	H_1	S_2
H_3	1.000	0.319	-0.298	-0.771
H_2	0.319	1.000	-0.105	-0.558
H_1	-0.298	-0.105	1.000	0.672
S_2	-0.771	-0.558	0.672	1.000